Int J Adv Manuf Technol (2015) 80:1689–1700
DOI 10.1007/s00170-015-7055-9

ORIGINAL ARTICLE

Effects of processing parameters on the surface quality of square section die-less spinning

Z. Jia[1] · Z. R. Han[1] · Q. Xu[1] · W. F. Peng[2] · Q. M. Kong[1]

Received: 2 November 2014 / Accepted: 18 March 2015 / Published online: 24 April 2015

Abstract In view of the importance of the surface quality in the application to the square section die-less spinning, the effects of several key parameters which include roller path, half-cone angle, and roller nose radius on the surface quality are investigated. Through the geometric model of residual height, the effect law of the roller path is obtained: the surface quality increases with the decrease of the axial distance of two adjacent slices. Then the finite element model of the square section die-less spinning is established, and the normal force and axial strain states in the deforming process are adopted to predict the relationship between the surface quality and the half-cone angle. Combined with the residual height model and finite element analysis, the roller nose radius' effect on the surface quality is also obtained. Enlargement of the two parameters can improve the surface quality. All the analysis results are verified by the surface waviness test of the specimens from the workpiece after spinning.

Keywords Square section die-less spinning · Surface quality · Roller path · Half-cone angle · Roller nose radius

✉ Z. R. Han
hanren888@163.com

[1] Key Lab of Fundamental Science for National Defense of Aeronautical Digital Manufacturing Process, Shenyang Aerospace University, Shenyang 110136, China

[2] Zhejiang Provincial Key Lab of Part Rolling Technology, Ningbo University, Ningbo 315211, China

1 Introduction

Spinning is one of plastic-forming technologies to produce shell parts from flat sheet or tubular blanks. By considering the net shape, many traditional cutting methods are replaced by spinning. The local contact between the roller and the blank makes the forming force much smaller than that in conventional press processing. Thus, spinning has been widely utilized in aviation, aerospace, and automotive industries [1]. From the last century, many scholars have conducted basic researches on regular circular cross-section spinning, for example, Kang et al. investigated the deformation mode of conventional spinning from sheet billet and found out that the wall thickness in the deformed area coincided well with the sine law and mandrel was not essential for the shear spinning [2]. Molladavoudi et al. studied the thickness reduction effects on spinning accuracy of aluminum 7075-O and found that the increment of thickness reduction has an adverse effect on geometrical accuracy and surface roughness [3].

Besides of these investigations of regular spinning process, some complex abnormal shape spinning was also derived and investigated. Gao et al. tested an ellipse spinning on their newly designed device and described the distribution of its wall thickness [4]. Xia et al. formed a cup shape by one-path deep drawing spinning and illustrated the effects of the parameters on the formability [5]. After that, Xia et al. proposed a non-axisymmetrical tube spinning process and investigated the stress, strain, and spinning forces of this process [6, 7]. The distributions of the force are not uniform around the circumferential direction, and the inhomogeneous stress will lead to forming defects. Then Bai

et al. simulated the power-spinning process of thin-walled shell with hoop inner rib and acquired the distribution of thickness and stress and the variations of spinning force in forming process at the same time [8]. Huang et al. analyzed the influence of material parameters on splitting spinning of aluminum alloy by FEM as follows: the average deviation angle of upper surface increases with the increase of yield stress and the decrease of hardening exponent and elastic modulus; the average deviation angle of lower surface increases with the decreased yield stress, hardening exponent, and elastic modulus [9, 10]. And then the forming characteristics of the splitting spinning were also described by Huang et al. [11]. Jiang et al. investigated the spinning process of thin-walled tubular part with longitudinal inner ribs. In their researches, multi-pass spinning and ball-shape roller were adopted, and the investigation results indicated that increasing the size of the ball contributed greatly to the stable flow of the metal as well as the formability of the inner ribs, but too large a ball led to the poor surface finish of the spun part; multi-pass spinning can guarantee the formability of the inner ribs [12, 13]. Shimizu obtained the elliptical cone-shaped products through synchronous spinning, but in his research, a mandrel with accordant shape was required [14]. Music et al. designed and manufactured a seven-axis machine and used it to form some axisymmetric parts by replacing the mandrel with three rollers [15]. The spinning of "Tripode" and "Pagoda" shape workpiece were simulated by Awiszus and Härtel, then experiments were carried out to verify the simulation results [16]. Sekiguchi and Arai investigated the oblique shear spinning and tried to control the wall thickness distribution after spinning [17]. Zhang et al. developed an accurate and effective three-dimensional (3D) FE model to improve the forming qualities of the large ellipsoidal heads formed by power spinning [18]. Xia et al. analyzed the spinning force of the triangular cross-section spinning compared to the conventional spinning [19]. The investigations above are focused on wall thickness distribution, stress-strain field, and spinning force but few reports approach the surface quality of irregular shape spinning, especially square section spinning.

The square section cone is shown in Fig. 1. It is like a pyramid with upper tip cut off and usually used as the shell parts of motors, lamps, and other devices. By traditional processing method, deep drawing is adopted to produce the square cone. But this method easily leads to fold defects experiencing complex manufacturing process and long preparation cycle. As a result, some scholars developed spinning method for the square section cone [14, 19] in which a modified mandrel die is needed with the shape corresponding to the square section cone. This will also bring in long preparation cycle and not suit the frequent changes of the parameters in the product development phase. Although die-less square section spinning is very flexible, it may cause surface quality problem due to lack of support from the mandrel. Several years ago, Elkhabeery et al. studied the influence of tool geometry and spinning parameters on the surface quality in the spinning process of cylindrical aluminum cups. In their study, the decrease of both roller angle and feed rate and the increase of roller nose radius could improve the surface quality [20]. The surface roughness of shear spinning was forecasted by Chen et al. [21]. They specialized in the effects of over-roll thickness on cone surface roughness [22] and deduced the regression equations for outer and inner surface roughness through a lot of test data. But all investigations above directed only at conventional shear spinning, and the mandrel was used in the experiments that may cause different results from the die-less one. Kwiatkowski et al. illustrated the fundamentals of controlling surface quality during die-less necking spinning process and showed that a high value of the round-off radius can reduce the surface waviness [23]. But unfortunately, their spinning object was tube. Square section die-less spinning is a very complicated plastic-forming process, and the contacting and force states between the roller and workpiece are different from conventional spinning; this will lead to different surface roughness. Because surface quality is directly related to the application of the square section cone, it is of paramount importance to unveil the influences of several key parameters on the surface quality.

2 Effect of roller path

2.1 Theoretical analysis

2.1.1 Density of contacting points

The basic principle of the square section spinning is as follows: Firstly, dividing the cone into many slices whose profile is square; secondly, the contacting point of the roller and workpiece moves from the upper slice to the lower one when the spindle rotates 45° with the workpiece. The moving path is the contacting line between the midpoint of upper square boundary and the endpoint of the lower one on the same side as shown in Fig. 2. Moreover, the position of the roller must correspond to the rotation angle of the workpiece strictly. In

our previous study [24], the radial roller path of the square section cone spinning was deduced. The formula is shown as

$$\frac{\frac{r_0\cos\theta_x}{\cos(\theta_x+\theta_1)}-\frac{r_0\cos\theta_x}{\cos(\theta_x+\theta_1+\Delta\theta)}}{v_x}=\frac{\Delta\theta}{360}\times\frac{1}{s} \tag{1}$$

Where, v_x is radial velocity of the roller, s is rotation speed of the spindle, r_{t1} is the radial distance between the roller contacting point and the rotation center O at the moment t_1 (the length of $\overline{OA}$), and r_{t2} is the radial distance between the roller contacting point and the rotation center O at the moment t_2 (the length of $\overline{OB}$). θ_1 is the angle which has been rotated by the spindle in the first 45° of the square shape. θ_x is a transition angle and expressed as

$$\theta_x=\arctan\left(\frac{\Delta r}{(r_0+\Delta r)\cot 45}\right) \tag{2}$$

Where Δr is the radial incremental step size in every rotation round. All the geometry dimensions above are illustrated in Fig. 2b.

According to the small value of θ_x, the axial roller path can be expressed as

$$\frac{\Delta Z_{t1}}{\Delta Z}=\frac{\tan(\theta_x+\theta_1)}{\tan(\theta_x+45)} \tag{3}$$

Or

$$\frac{\Delta Z_{t2}}{\Delta Z}=\frac{\tan(\theta_x+\theta_1+\Delta\theta)}{\tan(\theta_x+45)} \tag{4}$$

Where ΔZ is the axial distance of two adjacent slices. And the ratio of ΔZ and Δr can be used to determine the half square section cone angle α (Fig. 3).

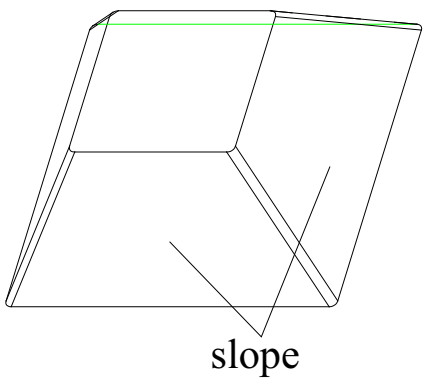

Fig. 1 Schematic diagram of square section cone

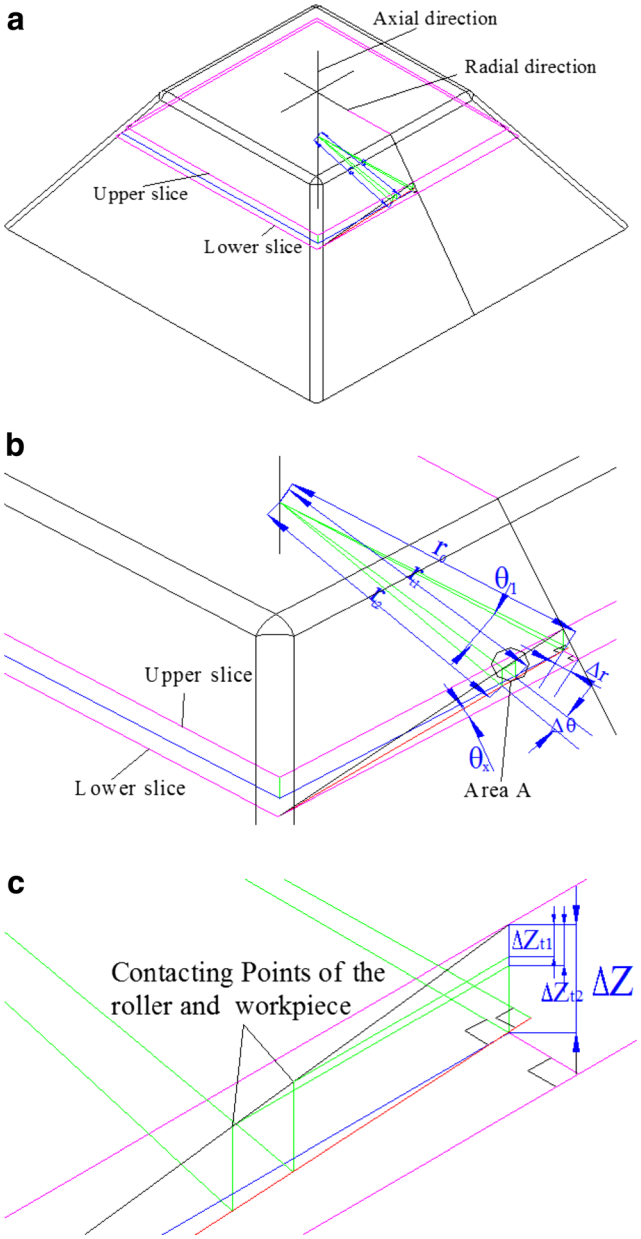

Fig. 2 Diagram of the roller path. **a** The whole cone. **b** Local amplification figure of two slices. **c** Local amplification figure of area A

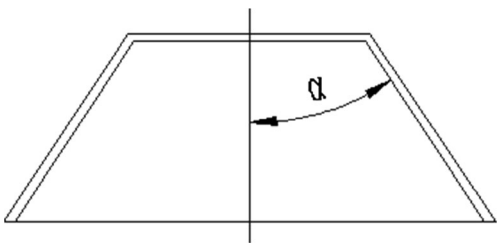

Fig. 3 Schematic diagram of the half-cone angle

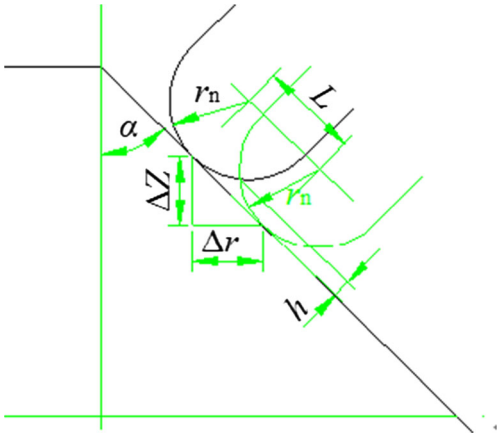

Fig. 4 Residual height on the symmetry plane of the slope

And

$$\tan\alpha = \frac{\Delta r}{\Delta Z} \tag{5}$$

When half-cone angle α is constant, the density of the slices increases with the diminution of ΔZ. According to trigonometric functions, smaller ΔZ results in smaller θ_x, and Eqs. (3) and (4) can be approximated into

$$\frac{\Delta Z_{t1}}{\Delta Z} = \tan\theta_1 \tag{6}$$

$$\frac{\Delta Z_{t2}}{\Delta Z} = \tan(\theta_1 + \Delta\theta) \tag{7}$$

Make a subtraction of Eqs. (4) from (5), there is

$$\frac{\Delta Z_{t2} - \Delta Z_{t1}}{\Delta Z} = \tan(\theta_1 + \Delta\theta) - \tan\theta_1 \tag{8}$$

From Eq. (6), we can also get that the distance between the contacting points will decrease with ΔZ. More contacting points imply the route in which the roller rotated with the workpiece is closer to a straight line. On the contrary, the route will be a curve. Hence, ΔZ can only be set to be a small value.

Table 1 Parameters of spinning experiment

Working conditions	Roller feed speed F_t/mm/min	Half-cone angle α/°	Roller nose radius /mm	ΔZ/mm
A	5000	45	2	0.09
B	8000	45	2	0.09
C	11,000	45	2	0.09
D	8000	30	2	0.09
E	8000	60	2	0.09
F	8000	45	8	0.09
G	8000	45	2	0.3

2.1.2 Residual height on the symmetry plane of the slope

In spinning process, when the spindle rotates 360° with the blank, a metal spike will be formed by the roller on the same slope of the square section cone. The height of the residual spike can stand for the surface quality in one way. Figure 4 is the schematic diagram of the residual height of the spike formed in one rotation round on the symmetry plane of the slope.

From Fig. 4, the residual height h can be expressed as

$$h = r_n - \sqrt{r_n^2 - \frac{L^2}{4}} \tag{9}$$

$$L = \sqrt{\Delta Z^2 + \Delta r^2} \tag{10}$$

Where L is the length of the contacting points between the roller and the workpiece on the symmetry plane of

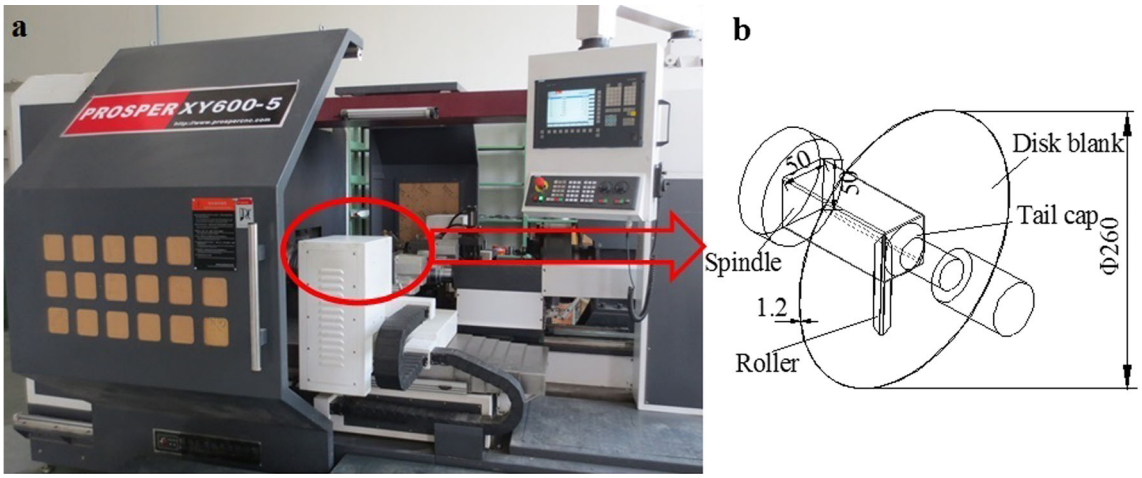

Fig. 5 **a** PS-CNCSXY 5-axis CNC spinning machine overall view. **b** Schematic diagram of the clamping for square section die-less spinning

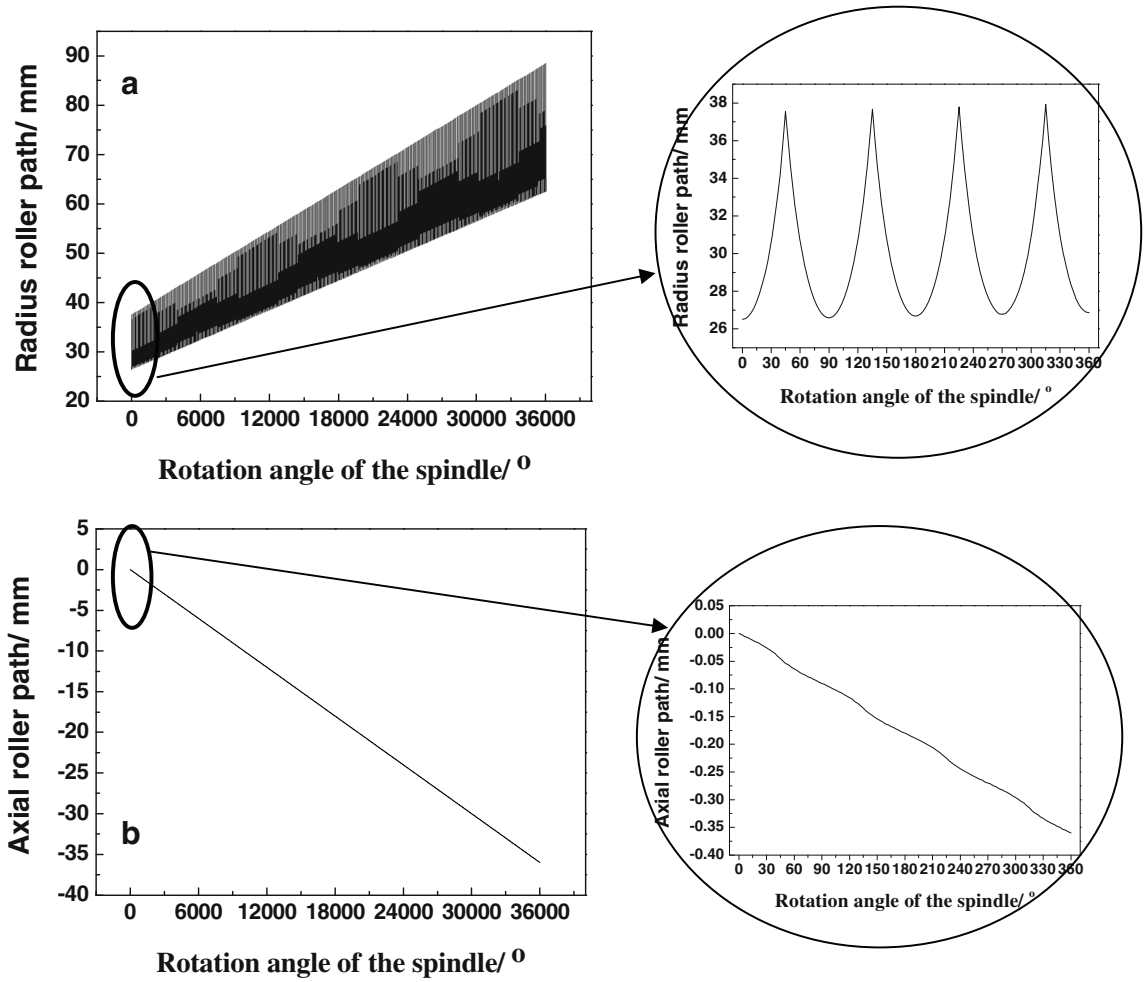

Fig. 6 Roller path adopted in working condition A. **a** Radial roller path. **b** Axial roller path

the slope in one rotation round, and r_n is the radius of the roller nose.

It can be found that from Eq. (7), h increases with L. If the half-cone angle α is kept constant, the residual height will go up along with the rise of ΔZ or Δr. Larger residual height means the waviness is obvious according to the geometrical relationship. So, small ΔZ (or Δr) is beneficial to the surface quality.

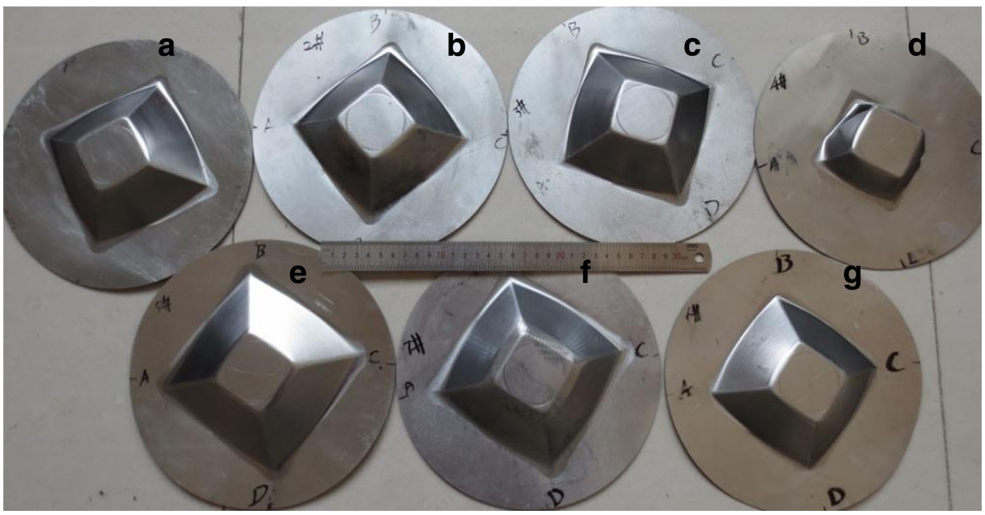

Fig. 7 Spun workpieces of all the working conditions in Table 1

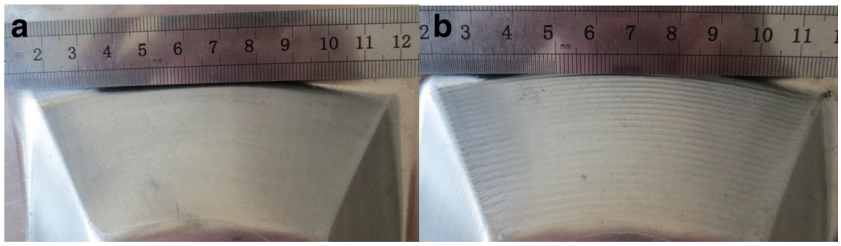

Fig. 8 Cone outer surface in working conditions B and G. **a** Working condition B. **b** Working condition G

2.2 Experimental verification

In order to verify the above analysis, a contrastive spinning experiment was carried out on PS-CNCSXY 5-axis CNC spinning machine as shown in Fig. 5. The parameters of the experiment are listed in Table 1.

Figure 5b is a schematic diagram of the clamping for square section die-less spinning. The diameter and thickness of the sheet blank are 260 and 1.2 mm, respectively, and its material is 6061 aluminum alloy. The example of the roller path adopted in working condition A is illustrated in Fig. 6.

The spun workpieces of all the working conditions in Table 1 are shown in Fig. 7.

Figure 8 shows the cone outer surface of working conditions B and G comparatively. It can be obviously found that the waviness on the surface of working condition B is much shallower than that in working condition G. This means that smaller ΔZ always contributes to a better surface quality. And then the theoretical analysis for the effect of ΔZ is verified.

3 Effect of the half-cone angle

3.1 Analysis by modeling

3.1.1 Finite element modeling

Firstly, based on the previous theoretical analysis, the half-cone angle depends on the ratio of ΔZ and Δr. In order to eliminate the influence of the roller path, the same residual heights are ensured in working conditions B and E. So there is

$$\Delta r_{\mathrm{E}} = \frac{\Delta r_{\mathrm{B}} \cos 30}{\cos 45} \tag{11}$$

Where, Δr_{B} and Δr_{E} are Δr in working conditions B and E.

Secondly, the 3D geometric models of the square section die-less spinning in working conditions B and E are established. With the addition of some boundary conditions, the finite element model is established by the dynamic explicit module of ABAQUS/Explicit, as shown in Fig. 9. The disk blank is defined as a 3D deformable solid body. The roller, square section spindle, and tail cap are constrained as rigid bodies. The roller can move on the radial and axial direction along the roller path and rotate around its central axis freely. A 20-KN force is applied on the tail cap along the axial direction. Both the tail cap and the spindle have their own revolving velocities matching the roller path. Both the friction coefficients between the tail cap and the disk blank and the spindle and disk blank are set to be 0.4. The friction coefficient between the roller and the disk blank is set to be 0.15, and the disk blank can rotate with the spindle due to friction. The elements C3D8R for "8-node linear brick, reduced integration, hourglass control" are used to mesh the disk blank for stable and efficient simulations.

Finally, the material used in the simulation and experiment is 6061 aluminum alloy (annealed). Its constitutive equation is obtained by Xia et al. [7]. The relationship between the true stress and strain is $Y=234\varepsilon^{0.26}$ and the mechanical properties of the metal are shown in Table 2.

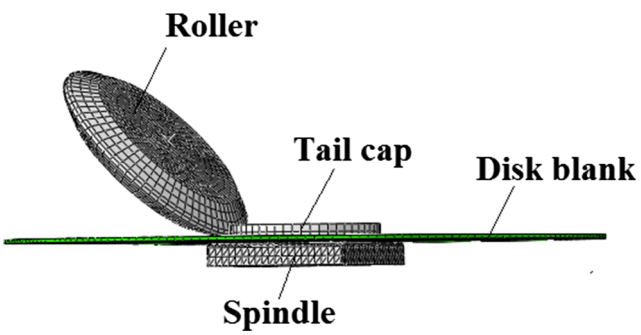

Fig. 9 Finite element model of square section die-less spinning

3.1.2 Simulation results and discussion

In order to validate the 3D-FE model of the square section die-less spinning process, the results from

Table 2 Mechanical properties of 6061 aluminum alloy (annealed)

Elastic modulus E (MPa)	67,308
Poisson's ratio υ	0.33
Yield strength σ_s (MPa)	51.59
Tensile strength σ_b (MPa)	146.12

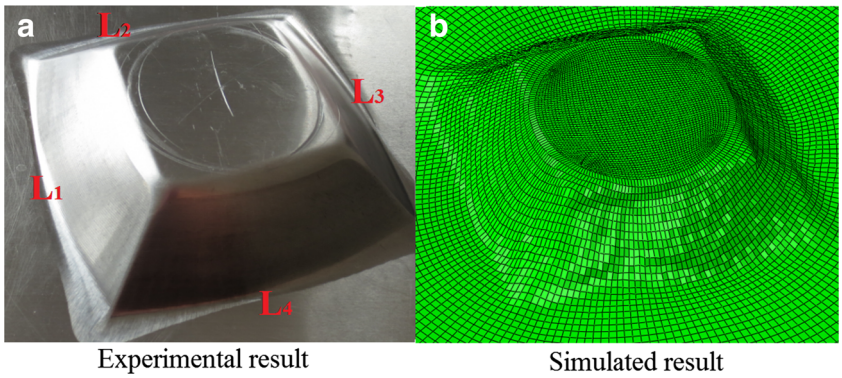

Fig. 10 Comparison of the **a** experimental and **b** simulated results

simulation and experiment based on the working condition B are compared in Fig. 10. The length of the square section edges when the axial height gets 18 mm is listed in Fig. 11. According to Fig. 10, the morphologies of the two results are similar. Both of them are tip-removed pyramid shape and the deviation of the edge length is less than 8 %. It is illustrated that numerical simulation results show a good agreement with experiments. So, it indicates the 3D-FE model built above is credible.

The normal force on the contacting zone between the roller and the slope can be deduced from the radial and axial forces which are obtained from the simulation result, and the relationship of the forces is illustrated in Fig. 12. The normal forces in working condition B and E are compared in Fig. 13, and in most of the process, it is greater in working condition B than that in working condition E due to the larger total deformation of working condition B. According to the arc shape of roller nose, the contacting areas in the working conditions B and E are the same with the identical indentation depth, so the smaller normal force will cause shallow indentation (because there is no mandrel in the die-less spinning process, the normal stress affects the wall thickness slightly). So, we can predict that the surface quality increases with the half-cone angle.

In another way, the surface quality is predicted again: According to cone shape of the workpiece, the main deformation occurs along the axial direction in the square section spinning process. So, the axial strain fields on the slopes of the workpiece in the working conditions B and E are inspected in Fig. 14. It can be found that the axial strain mainly presents as compressive strain, and in working condition B, it is bigger than that in working condition E with the same rotation round. This can be interpreted as that smaller half-cone angle leads to bigger deformation on the axial direction both in every rotation round and the whole spinning process. According to the conclusion of ref. [25]—"the spectral density of long wavelength components decrease during low-reduction rolling, while increase significantly during high-reduction rolling"; this means that a smooth surface was obtained for small reduction ring rolling process, meanwhile it also shows that a lower plastic strain is consistent with a better surface quality. Therefore, the surface quality is promoted by the bigger half-cone angle.

3.2 Verification by waviness test

Except working condition D (cracking as shown in Fig. 7), a test piece is cut from the trapezoidal slope

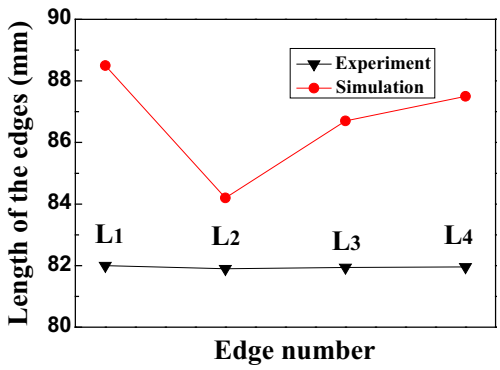

Fig. 11 Comparison of the edge length

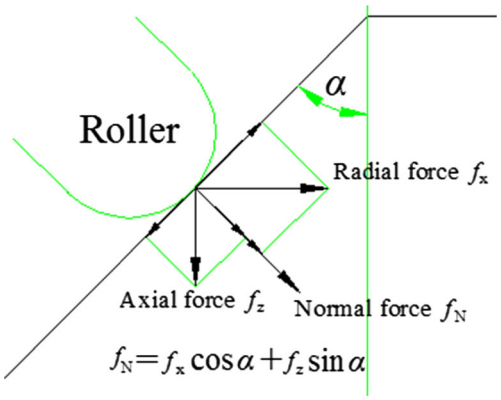

Fig. 12 Schematic diagram of the force on the contacting zone

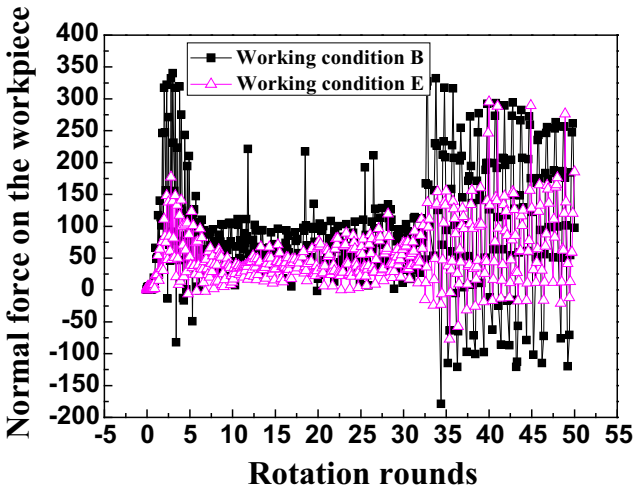

Fig. 13 Comparison of the normal force between the working conditions B and E

of the workpieces in working conditions A–G. Figure 15 illustrates the sampling position and the sizes of the sample. Three measuring courses on each test piece are selected randomly for the waviness W_a, and the measurement is carried out on the Alpha-step IQ surface profiler.

In order to evaluate the surface quality of the workpiece, the following definitions are done:

The maximum W_a of the three testing processes on one sample reflects the waviness of the slope.

The average value of 4 W_a from 4 slopes gives expression of the surface quality of the workpiece.

The W_a of working condition B and working condition E are shown in Fig. 16. From Fig. 16, it is found that the waviness of working condition B is bigger than that in working condition E both on each corresponding slope and the whole workpiece. The difference of the whole workpiece can be as large as 28.8 %. This means a larger half-cone angle is beneficial to obtaining smoother surface in square section die-less spinning process.

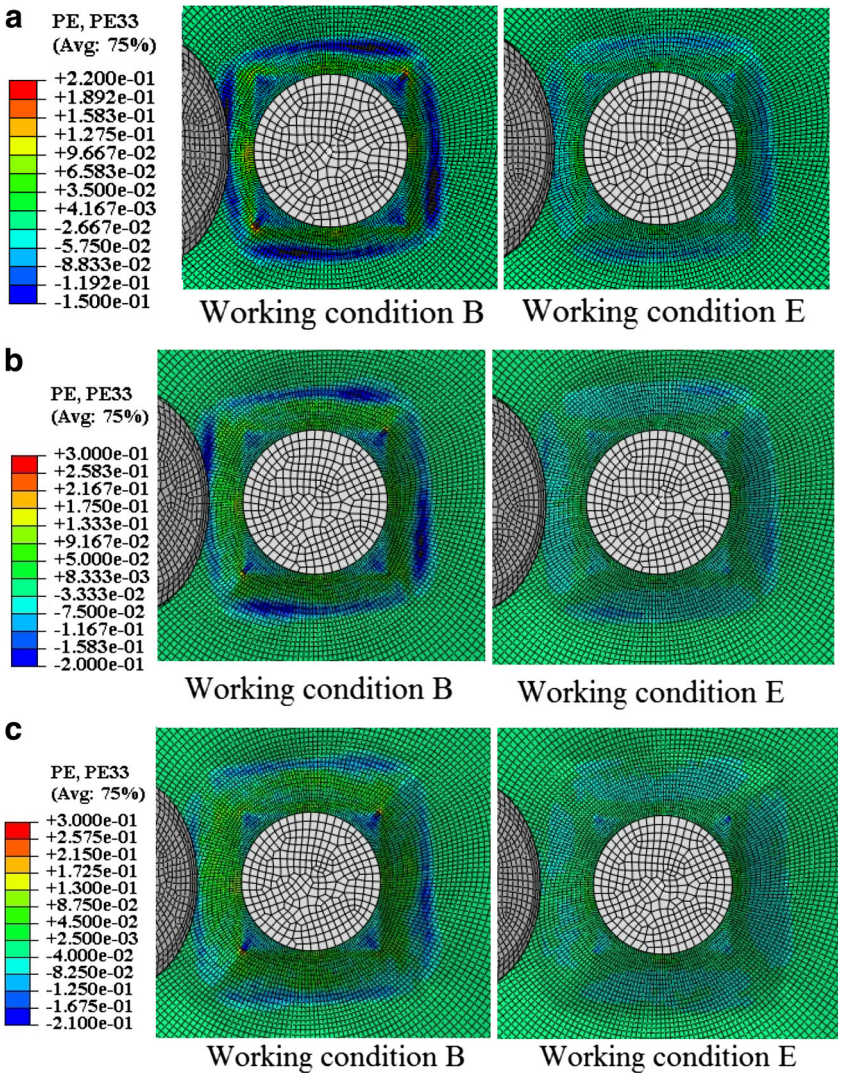

Fig. 14 Axial strain fields in the working conditions B and E in the spinning process. **a** Spindle rotation rounds 20. **b** Spindle rotation rounds 30. **c** Spindle rotation rounds 40

4 Effect of roller nose radius

4.1 Analysis by modeling

4.1.1 Geometric model of residual height

The geometric model of the residual height after spinning in one rotation round is deduced as Eq. (7). Take dh/dr_n from Eq. (7), the following derivative with respect to r_n is obtained:

$$\frac{dh}{dr_n} = 1 - \frac{r_n}{\sqrt{r_n^2 - \frac{L^2}{4}}} \tag{12}$$

Because the value of dh/dr_n is smaller than 0, the residual height h grows up as the roller nose radius r_n degrades in Eq. (7). So, from the simple mathematical derivation, it is found that bigger roller nose radius improves the surface quality.

4.1.2 Finite element analysis

The comparison of the normal forces in working conditions B and F is shown in Fig. 17. At the beginning, the normal force in working condition B is obviously larger than that in working condition F; five rotating rounds after that, the normal force in working condition F becomes greater. This fluctuation phenomenon of the force is caused by the different initial gap between the arc top of the roller nose and the blank. Then the normal forces tend to the same. With bigger radius roller nose, the contacting area in the working condition F is larger than that in working condition B with the same indentation depth. So, deeper indentation will be obtained from the working condition B with the same normal force but smaller contacting area. Hence, worse surface quality is predicted to be obtained in the working condition with smaller roller radius.

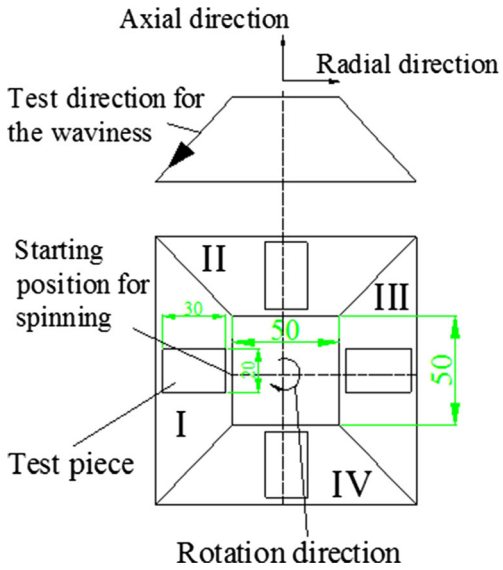

Fig. 15 Cutting position and sizes of the sample for waviness test

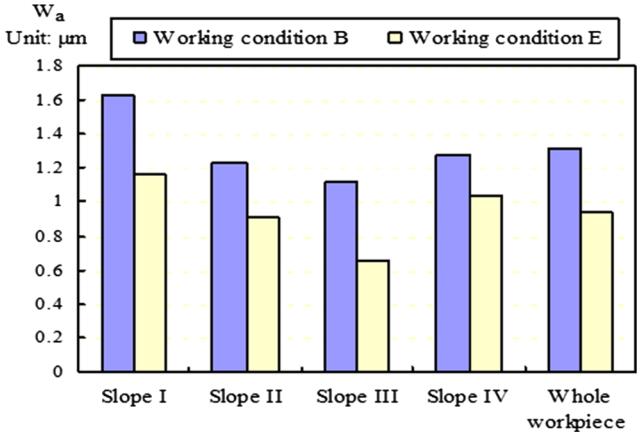

Fig. 16 W_a of working condition B and working condition E

The axial strain field is adopted to evaluate the surface quality here too, as shown in Fig. 18. It can also be found that the axial strain in working condition B is the bigger one at the same spinning process due to smaller contacting area between the roller and the workpiece under the same resistance from the disk blank. The surface quality is improved by bigger roller nose radius, which also proves the previous analysis.

4.2 Verification by waviness test

Figure 19 illustrates the test values of waviness W_a in working conditions B and F. The data in Fig. 19 also display that the waviness in working condition B is bigger than that in working condition E with each slope

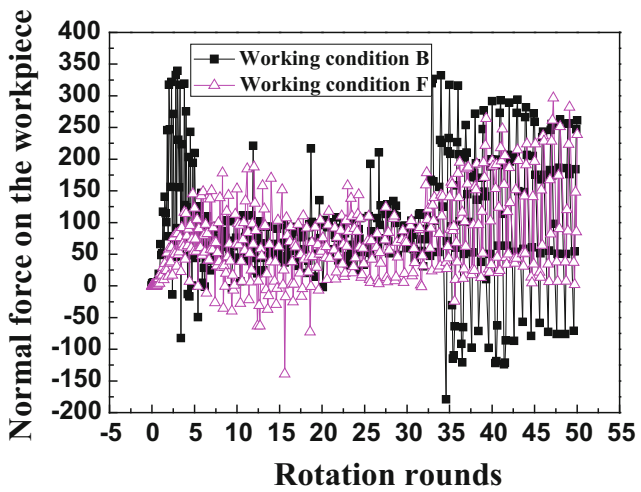

Fig. 17 Comparison of the normal force between the working conditions B and F

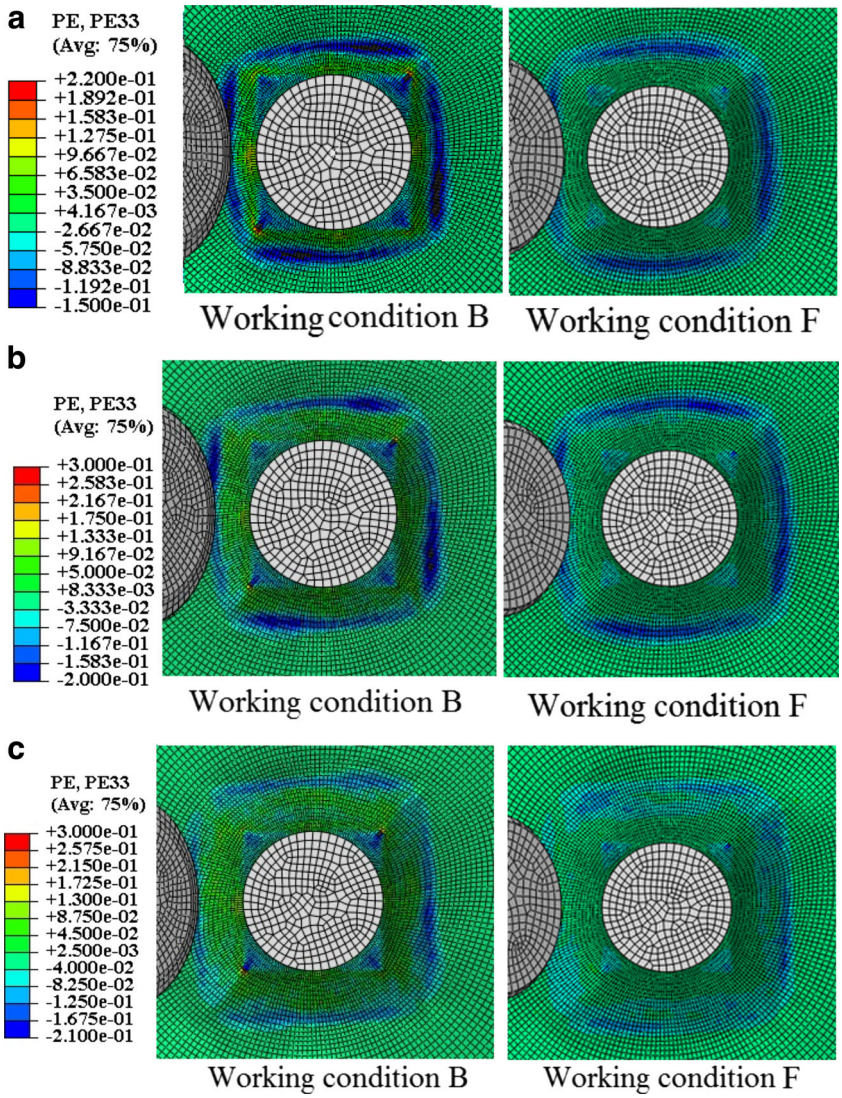

Fig. 18 Axial strain fields in the working conditions B and F in the spinning process. **a** Spindle rotation rounds 20. **b** Spindle rotation rounds 30. **c** Spindle rotation rounds 40

and the whole workpiece. The deviation of whole workpiece is 44.4 %. Hence, the surface quality is improved with the increase of the roller nose radius for square section die-less spinning.

5 Effect of roller feed speed

The waviness W_a in working conditions A, B, and C is illustrated in Fig. 20. The difference between them is not so big

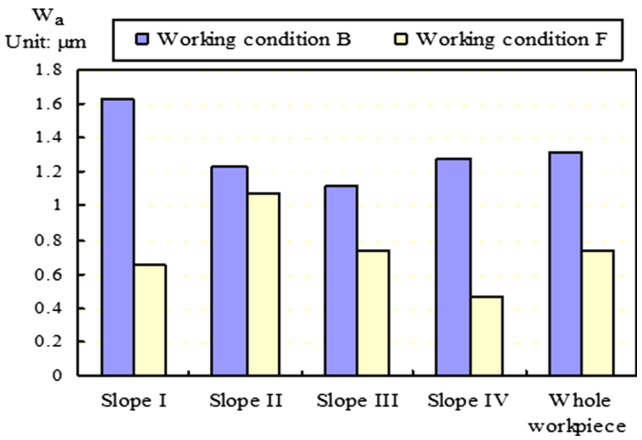

Fig. 19 W_a in working conditions B and F

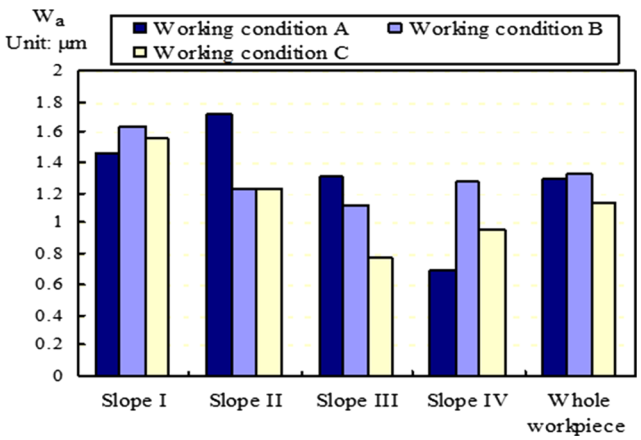

Fig. 20 W_a in working conditions A, B, and C

and the maximum deviation of W_a for the whole workpiece is 14 %. The roller feed speed affecting on the surface quality is not obvious. The reason for this is that the roller must move forward and backward on the radial direction in order to form the square section. The stroke in one direction is about 12–50 mm, and one-way transport time for the roller is 0.065–0.6 s (if the roller feed is reduced to a very low value such as 500 mm/min, the rotated speed of the spindle which needs match will decrease to 5 r/min and exceeds the low speed limit of the spindle motor). This means the operator of the spinning machine must achieve a reversal in such a short period, and it is not enough to speed up the movement of the roller by the servo motor. So, the effect law of the feed speed does not perform obviously.

6 Conclusions

The effects of the roller path, half-cone angle, and roller nose radius on surface quality of square section die-less spinning are investigated through mathematics and finite element analysis. The main conclusions are as follows:

1. The equation of the roller path is further deduced by mathematics method, and the geometric model of the residual height on the symmetry plane of the slope is derived to study the influence of the roller path on the surface quality. And then the conclusion that small ΔZ (or Δr) is beneficial to the surface quality is verified experimentally. The reason for is that the residual height will go down with the decrease of ΔZ or Δr.
2. Under the condition of the same residual height, the finite element method is adopted to predict the effect of the half-cone angle on the surface quality comparatively. Through the analysis of the normal force and axial strain in the square section die-less spinning process and waviness test, it is found out that there is a greater normal force on the smaller half-cone angle slopes due to the larger total deformation. This leads to shallower indentation and means the surface quality increases with the half-cone angle. This conclusion is verified by the experiment.
3. The effect of the roller nose radius on the surface quality formed by the square section die-less spinning is obtained from the geometric model of residual height and finite element analysis. Smaller roller nose radius causes deeper indentation and residual height on the surface of the workpiece with the same normal force, and higher axial plastic strain is obtained. At last, it is also confirmed by the waviness test that the surface quality is improved by bigger roller nose radius.
4. According to the response accuracy of the spinning machine, the effect law of the feed speed cannot be distinguished obviously. In the future, more advanced methods are needed to investigate it.

Acknowledgments This work was financially supported by the Open Foundation of Zhejiang Provincial Key Lab of Part Rolling Technology, China (No. ZKL-PR-20030), and authors would like to express their gratitude.

References

1. Music O, Allwood JM, Kawai K (2010) A review of the mechanics of metal spinning. J Mater Process Technol 210(1):3–23
2. Kang DC, Gao XC, Meng XF, Wang ZH (1999) Study on the deformation mode of conventional spinning of plates. J Mater Process Technol 91(1):226–230
3. Molladavoudi HR, Djavanroodi F (2011) Experimental study of thickness reduction effects on mechanical properties and spinning accuracy of aluminum 7075-O, during flow forming. Int J Adv Manuf Technol 52(9–12):949–957
4. Gao XC, Kang DC, Meng XF, Wu HJ (1999) Experimental research on a new technology—ellipse spinning. J Mater Process Technol 94(2):197–200
5. Xia Q, Shima S, Kotera H, Yasuhuku D (2005) A study of the one-path deep drawing spinning of cups. J Mater Process Technol 159(3):397–400
6. Xia QX, Cheng XQ, Hu Y, Ruan F (2006) Finite element simulation and experimental investigation on the forming forces of 3D non-axisymmetrical tubes spinning. Int J Mech Sci 48(7):726–735
7. Xia QX, Xie SW, Huo YL, Ruan F (2008) Numerical simulation and experimental research on the multi-pass neck-spinning of non-axisymmetric offset tube. J Mater Process Technol 206(1–3): 500–508
8. BAI Q, YANG H, Zhan M (2008) Finite element modeling of power spinning of thin-walled shell with hoop inner rib. Trans Nonferrous Metals Soc China 18(1):6–13
9. Huang L, Yang H, Zhan M (2008) 3D-FE modeling method of splitting spinning. Comput Mater Sci 42(4):643–652
10. Huang L, Yang H, Zhan M, Hu LJ (2008) Numerical simulation of influence of material parameters on splitting spinning of aluminum alloy. Trans Nonferrous Metals Soc China 18(3):674–681
11. Huang L, Yang H, Zhan M, Hu L (2009) Forming characteristics of splitting spinning based on the behaviors of roller. Comput Mater Sci 45(2):449–461
12. Jiang S, Ren Z, Li C, Xue K (2009) Role of ball size in backward ball spinning of thin-walled tubular part with longitudinal inner ribs. J Mater Process Technol 209(4):2167–2174
13. Jiang SY, Zheng YF, Ren ZY, Li CF (2009) Multi-pass spinning of thin-walled tubular part with longitudinal inner ribs. Trans Nonferrous Metals Soc China 19(1):215–221
14. Shimizu I (2010) Asymmetric forming of aluminum sheets by synchronous spinning. J Mater Process Technol 210(4):585–592
15. Music O, Allwood JM (2011) Flexible asymmetric spinning. CIRP Ann Manuf Technol 60:319–322
16. Awiszus B, Härtel S (2011) Numerical simulation of non-circular spinning: a rotationally non-symmetric spinning process. Prod Eng 5(6):605–612
17. Sekiguchi A, Arai H (2012) Control of wall thickness distribution by oblique shear spinning methods. J Mater Process Technol 212(4):786–793
18. Zhang J, Zhan M, Yang H, Jiang Z, Han D (2012) 3D-FE modeling for power spinning of large ellipsoidal heads with variable thicknesses. Comput Mater Sci 53(1):303–313

19. Xia QX, Lai ZY, Long H, Cheng XQ (2013) A study of the spinning force of hollow parts with triangular cross sections. Int J Adv Manuf Technol 68(9–12):2461–2470
20. El-Khabeery MM, Fattouh M, El-Sheikh MN, HAMED OA (1991) On the conventional simple spinning of cylindrical aluminum cups. Int J Mach Tools Manuf 31(2):203–219
21. Chen MD, Hsu RQ, Fuh KH (2001) Forecast of shear spinning force and surface roughness of spun cones by employing regression analysis. Int J Mach Tools Manuf 41(12):1721–1734
22. Chen MD, Hsu RQ, Fuh KH (2005) Effects of over-roll thickness on cone surface roughness in shear spinning. J Mater Process Technol 159:1–8
23. Kwiatkowski L, Tekkaya AE, Kleiner M (2013) Fundamentals for controlling thickness and surface quality during dieless necking-in of tubes by spinning. CIRP Ann Manuf Technol 62(1):299–302
24. Jia Z, Han ZR, Xu Q, Peng WF (2014) Numerical simulation and experiment study on hollow spinning process for square cross-section cone. Int J Adv Manuf Technol 75(9–12):1605–1612
25. Ma B, Tieu AK, Lu C, Jiang Z (2002) An experimental investigation of steel surface characteristic transfer by cold rolling. J Mater Process Technol 125–126(3):657–663